Isolation design of a 14.4kV, 100kHz transformer with a high isolation voltage (115kV)

Michael Jaritz, Jürgen Biela
Laboratory for High Power Electronic Systems,
ETH Zurich, Physikstrasse 3, CH-8092 Zurich, Switzerland
Email: jaritz@hpe.ee.ethz.ch

***Abstract*—In this paper, the isolation design procedure of a 14.4kV output voltage, 100kHz transformer with an isolation voltage of 115kV using Litz wire is presented. For designing the isolation, a comprehensive design method based on an analytical maximum electrical field evaluation and an electrical field conform design is used. The resulting design is verified by long and short term partial discharge measurements on a prototype transformer.**

***Keywords*— High voltage, high frequency transformer; isolation design**

I. Introduction

For the new linear collider at the European Spallation Source (ESS) in Lund, 2.88MW pulse modulators with pulsed output voltages of 115kV and pulse lengths in the range of a few milliseconds are required (pulse specifications see Tab.I). For generating these pulses, a long pulse modulator based on a modular series parallel resonant converter (SPRC) topology has been developed [1]. This converter is operated at high switching frequencies (100kHz-110kHz) to minimize the dimensions of the reactive components and the transformer. To achieve the required output voltage of 115kV, 8 SPRC basic modules each with an output of 14.4kV are connected in series [2], see Fig.1. Due to the series connection of the SPRC basic modules, the insulation of the last oil isolated transformer in the row has to withstand the full pulse voltage.
In the literature several approaches are presented for designing a high voltage, high frequency transformer [3, 4, 5] with nominal output voltages between 50kV-60kV and a switching frequency of 20kHz. The transformer presented in [6] is designed with respect to an isolation voltage of 15kV, a nominal output voltage of 3.8kV and 3kHz operation frequency. In [7] the design is carried out for a nominal output voltage of 3kV, a switching frequency of 10kHz and provides partial discharge measurements for short term tests(1 min, test voltage 28kV). However, all of these transformers are either tested only under nominal field conditions [3]-[6] and/or no values for long term partial discharge measurements which are an essential life time key parameter for high voltage components are given [7]. In addition the isolation voltage of 115kV and the switching frequency range of 100kHz-110kHz exceed by far the designs in [3]-[7]. Therefore, in this paper an isolation design procedure for a 14.4kV nominal output voltage, 100kHz transformer with an isolation voltage of 115kV is given and verified by long term (60 min) nominal test voltage and short term (5 min) extended test voltage (up to 136%) partial discharge measurements.
In section II, an isolation design procedure which is part of a transformer optimization procedure is presented, which is used to design the transformer for ESS. Afterwards, in section

TABLE I: Pulse specifications

Pulse voltage	V_K	115 kV
Pulse current	I_K	25 A
Pulse power	P_K	2.88 MW
Pulse repetition rate	P_{RR}	14 Hz
Pulse width	T_P	3.5 ms
Pulse duty cycle	D	0.05
Pulse rise time (0..99 % V_K)	t_{rise}	150 µs
Pulse fall time (100..10 % V_K)	t_{fall}	150 µs

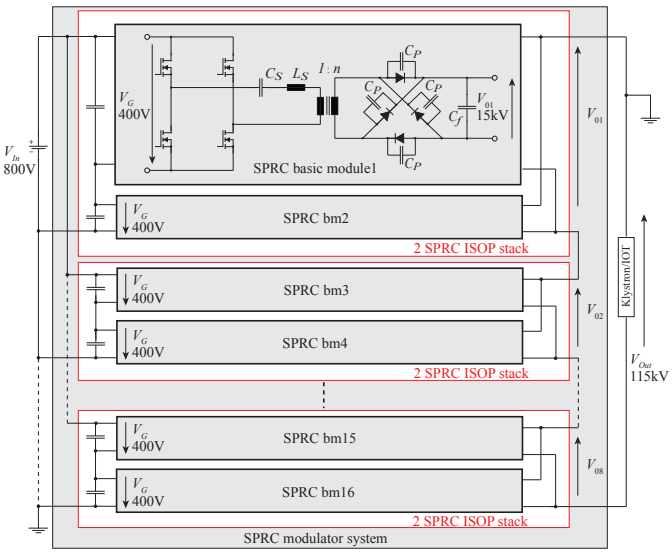

Fig. 1: SPRC modulator system with 2 SPRC basic modules forming an ISOP stack [2] and 8 of them are connected in series to achieve the required output voltage.

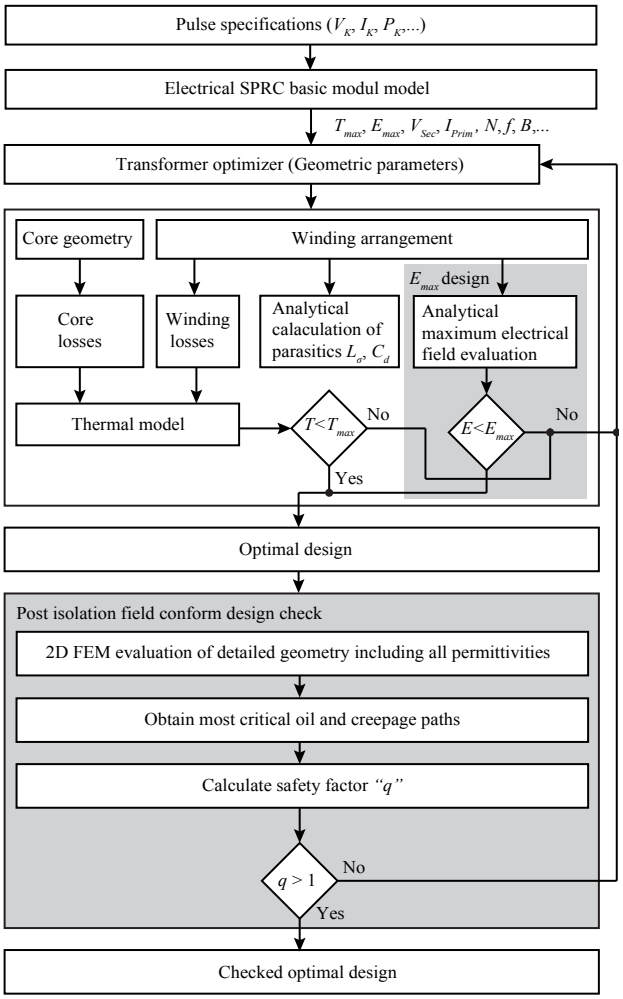

Fig. 2: Transformer optimization with integrated isolation design procedure (grayed shown areas).

III the resulting design is evaluated by long term nominal test voltage and short term over-voltage partial discharge measurements.

II. Isolation Design Procedure

Due to the high number of degrees of freedom during the transformer design process as for example the geometric parameters of the core or the windings, an optimization procedure has been developed for optimally designing the transformer (see Fig. 2) [1]. In the first step, an electrical model of the SPRC basic module determines the input parameters and constraints for the transformer optimization, for the given pulse specifications. Before the transformer design procedure is started, first a specific core and winding geometry has to be chosen. For the core geometry an E-type core is used. For the winding geometry, there are five basic winding configurations possible (Fig.3) which are investigated with respect to the maximum electrical field, lowest electrical energy per length W'_E and maximum wire to wire withstand voltage V_{WS} by varying the distance Δx. The standard and

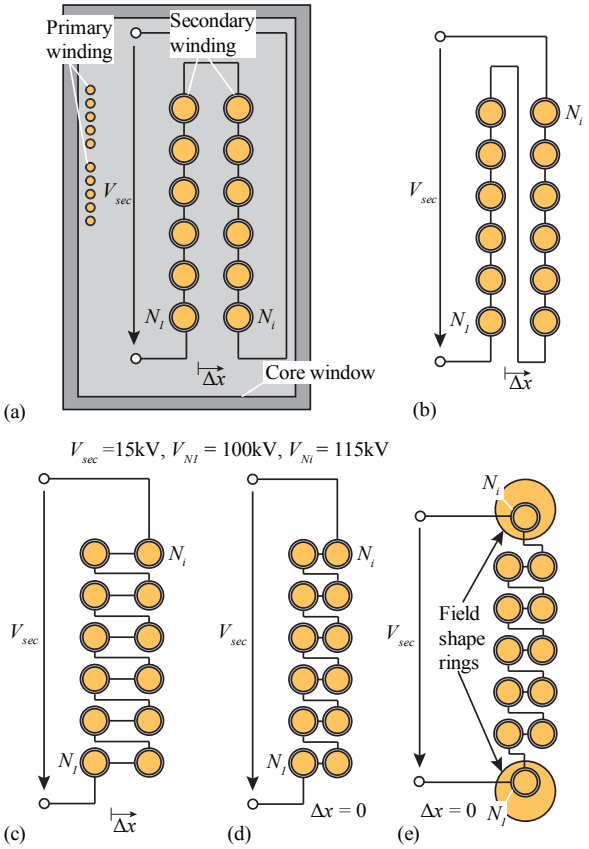

Fig. 3: Five basic winding configurations: (a) Standard winding, (b) flyback winding, (c) s-winding, (d) s-winding with $\Delta x = 0$, and (e) s-winding arrangement with field shape ring and $\Delta x = 0$.

the flyback winding configuration (see Fig.3(a) and (b)) lead to high E_{max}, W'_E and V_{WS} values [8]. The s-winding configuration (see Fig.3(c) and (d)) has the advantage of a minimum withstand voltage, but still high E_{max} values occur. Adding a field shape ring to Fig.3(d) results in the winding arrangement given in Fig.3(e). The first and the last turn of the winding are mounted inside field shape rings leading to a reduced E_{max}. Fig.4(a) and (b) show the electrical field distribution of the s-winding configuration with and without field shape rings. Comparing case (d) and (e) in Tab.II, the occuring peak field is reduced by 43.3%. The field shape rings are on the same potential as the respective turn and one

TABLE II: E_{max} evaluation results

Config.	Δx [mm]	E_{max} [kV/mm]	W'_E [mJ/m]	V_{WS} [kV]
(a)	6.1	16.53	435.22	V_{sec}
(b)	6.1	15.8	433.66	$V_{sec}/2$
(c)	2.1	15.96	401.28	$4V_{sec}/N_i$
(d)	0	16.11	385.86	$4V_{sec}/N_i$
(e)	0	11.24	461.64	$4V_{sec}/N_i$

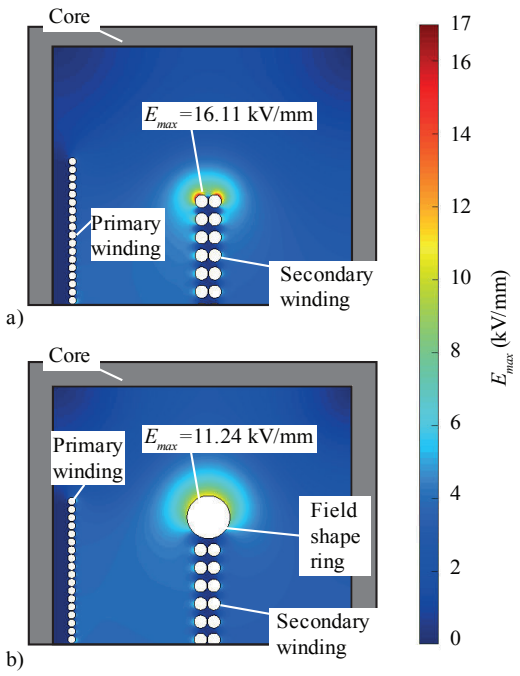

Fig. 4: (a) Maximum E-field of s-winding and (b) maximum E-field of s-winding with a field shape ring (10mm diameter) inside the core window.

end of the turn is soldered to the corresponding field shape ring, see Fig.5(d). Due to this arrangement the high frequency losses do not increase much because most of the load current is still conducted by the Litz wire and not by the field shaping ring. With the defined core and winding geometry (Fig.3(e)) all losses and parasitics are calculated and also the maximum electrical peak field is estimated. Afterwards, in a FEM based post design check a detailed model of the transformer is evaluated regarding oil gap widths and creepage paths.

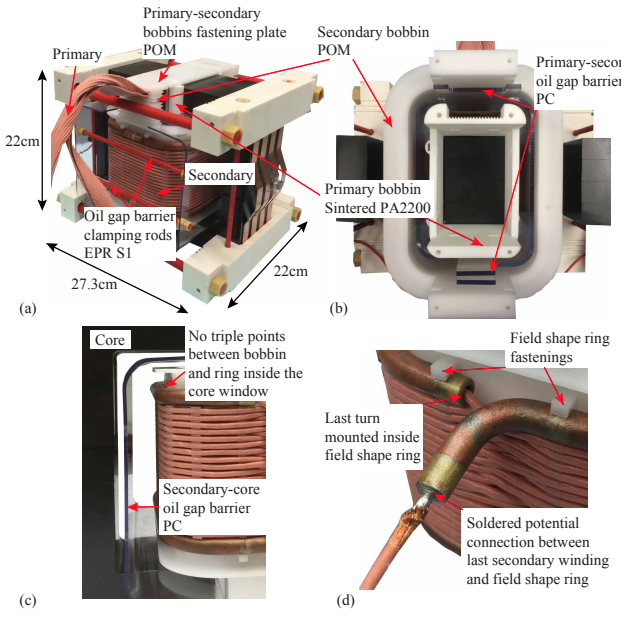

Fig. 5: (a) Transformer prototype (built by AMPEGON AG). (b) Top view of the transformer, which has no mountings between primary and secondary inside the transformer, (c) core window with oil gap barrier and (d) last turn mounted inside the field shape ring.

In the following the isolation design procedure (areas highlighted in gray in Fig.2) which can be divided into an analytical maximum electrical field evaluation and a FEM supported post isolation field conform design check are described more in detail.

A. *Evaluation of the maximum electrical field*

Due to the complexity of the transformer isolation structure, it is not computationally efficient to use a comprehensive analytical model of the transformer including all details as e.g. bobbins, winding fastenings and oil gap barriers (see Fig.5) in the optimization procedure. Instead an analytical maximum electrical field calculation is used, which is based on the image charge method [1] and allows a quick basic isolation design check considering the maximal electrical field which has to be below a certain constraint value (see Fig. 2). This method considers a single insolation material permittivity and is ≥ 7 times faster than FEM, because only a few points along the surface of the turn with the highest potential are evaluated to estimate the highest E_{max} value.

B. *FEM supported field conform design*

In the following, first, the material characteristic of the components are presented and afterwards the FEM supported field conform post design procedure is discussed. For the built prototype emphasis was put on the choice of proper insulation

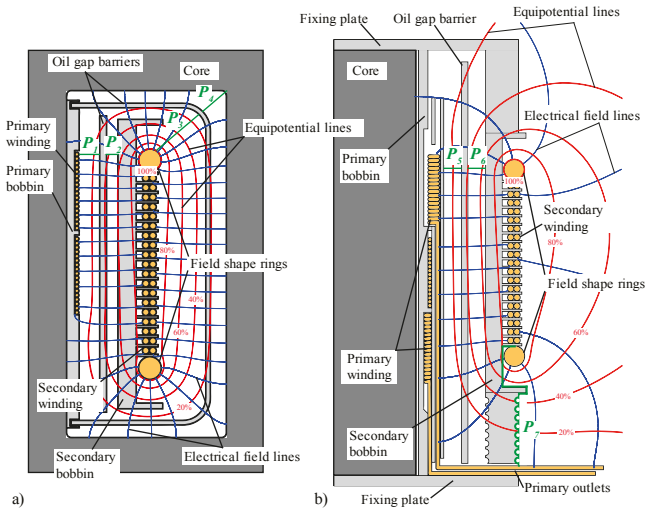

Fig. 6: Electrical field and potential distribution (a) inside the core window and (b) at the front side of the transformer with the considered oil (P_1-P_6) and creepage paths (P_7).

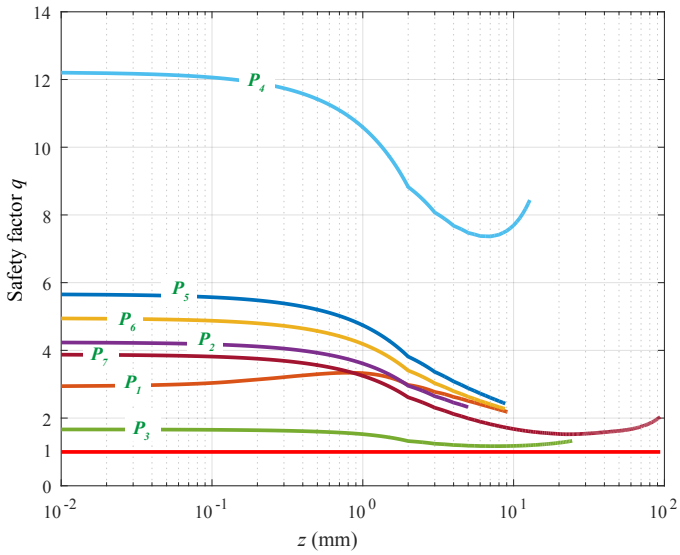

Fig. 7: Evaluated oil gap (P_1-P_6) and creepage paths (P_7). For a valid design all q curves have to be above 1.

materials (see Tab.III). The main insulation material is the transformer oil MIDEL7131 [9] with a relative permittivity of 3.2. All other insulation materials are chosen with respect to the transformer oil such that they have a similar permittivity to avoid local field enhancements at the boundary layer of different materials and maximum electrical strength.

Fig.5(a) shows the built transformer prototype, which has no mountings between the primary and the secondary bobbin inside the transformer in order to prevent creepage paths (see Fig.5(b)). The bobbins are fixed outside of the core window at the top and the bottom of the transformer, resulting in a longer creepage distance between the windings (see Fig.6(a) and (b)). The maximum field strength occurs at the field shape ring inside the core window. Hence, triple points [10] between the field shape rings and the secondary bobbin inside the core window should be avoided (see Fig.5(c)). Thus, all field shape ring fastenings are located in a region of weak E-field outside at the front of the secondary bobbin as can be seen in Fig.5(d). The primary bobbin is completely sintered of PA2200 material in a 3D printing process. This process allows complex designs but the resulting components are not void free [15], so this material is used only in non critical electrical field areas. The secondary bobbin is milled out of a single solid POM block

TABLE III: Material parameters

Material	**Permitivity**	**Electrical strength [kV/mm]**
POM [11]	3.5	50
PC [12]	3	30
PA2200 [13]	3.8	92
EPR S1 [14]	5	10
Material	**Permitivity**	**Breakthrough voltage [kV]**
MIDEL7131 [9]	3.2	75

to minimize voids and component intersections (see Fig.5(b)). Additionally, silk wrapped Litz-wire is used instead of foil so that no air bubbles are trapped beneath the foil.

An inappropriate design causes partial discharges as well as sliding discharges which can harm the isolation of the transformer permanently and lead to arcs between the windings or the core. Oil gap barriers between primary and secondary winding as well as between secondary winding and core are used to counter the decreasing electrical strength of long oil gaps due to the volume and the area effect [10]. Therefore, for long life times a proper isolation design is necessary and a detailed analysis of the electrical field distribution along long oil paths (P_1-P_6, see Fig.6(a) and (b)) and critical creepage paths (P_7, see Fig.6(b)) was carried out with the help of the Weidmann design curve method [16]. There, the ratio of oil design curves ($E_d(z)$) which are derived from homogenous electrical breakdown tests [17] and the averaged cumulated electrical field strength E_{avg} along certain path lenghts (z) is calculated, resulting in safety factor curves q [10].

$$E_{avg}(z) = \frac{1}{z}\int_0^z E(z')dz' \tag{1}$$

$$q = \frac{E_d(z)}{E_{avg}(z)} \tag{2}$$

$E(z')$ is the electrical field point at point z' and q has to be multiplied by 0.7 if used for creepage paths [10]. For a valid design the q's of all evaluated paths have to be above 1 (see Fig.7). With this method, isolation designs with homogenous as well as with strongly inhomogenous field distributions can be investigated. Finally, applying this method leads to an electrical field conform design, which means that the equipotential lines just have mostly tangential components along the surface of insulation boundaries, e.g. oil gap barriers (see Fig.6). Hence, the insulator is stressed mostly by the normal component of the electrical field and has its maximum electrical strength.

Tab.IV summarizes the optimization results of the transformer.

TABLE IV: Optimization results of the SPRC-basic module transformer.

V_{Sec}	14.4 kV	l	27.3 cm
I_{Prim}	1200 A	w	22 cm
f	100 – 110 kHz	h	22 cm
E_{max}	< 12 kV/mm		
# of cores		Type: Ferrite K2008	
16		U126/91/20	
Windings		Litz wire	
Primary Wndg.	2	18 x 405 x 0.071	
Secondary Wndg.	40	1125 x 0.071	

In the next section the isolation design is verified by partial discharge measurements.

III. Partial Discharge Measurements

For long life times it is not sufficient to know if the transformer withstands a certain voltage level without any

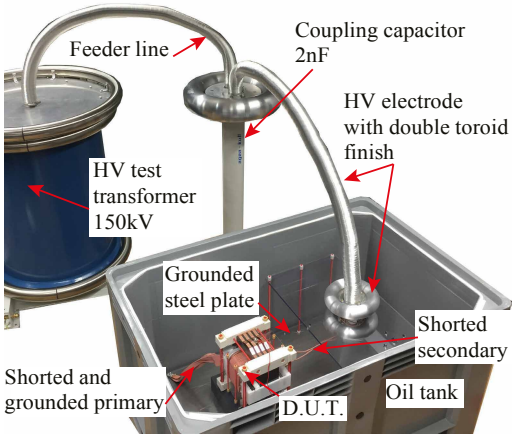

Fig. 8: Partial discharge measurement setup

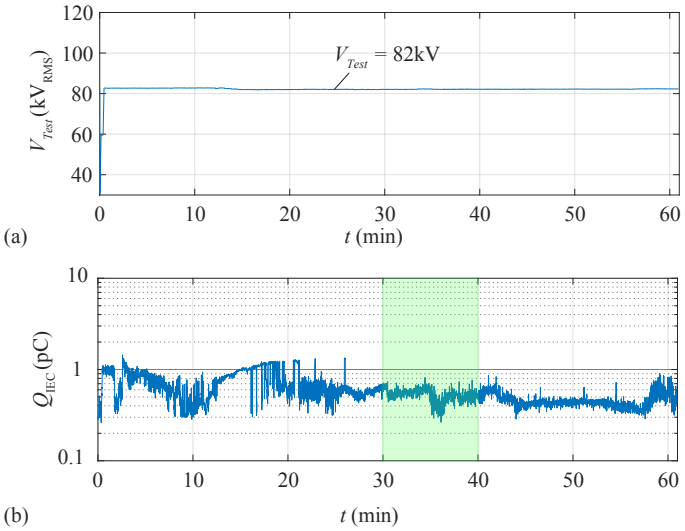

Fig. 9: (a) Applied stress voltage $V_{Test} = 82\,\mathrm{kV_{RMS}}$ with a test duration of 60min and (b) averaged measured partial discharges level Q_{IEC} which has been weighted considering [19]. The green interval is used for Fig.10

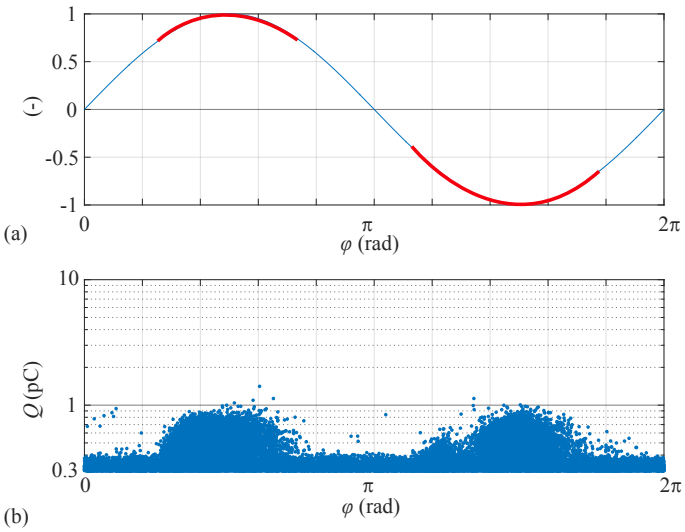

Fig. 10: (a) Red high lighted parts show the region of the normalized test voltage sinus where discharges mostly occur and (b) phase resolved non averaged partial discharges Q measured during the green time interval in Fig.9(b).

breakthroughs. It is also of high importance to know if the transformer is suffering from partial discharges. Such discharges can harm the insulation permanently during normal operation and may lead to serious failures. Therefore, in this section the results of comprehensive partial discharge tests are presented.

The isolation of a single SPRC basic module transformer has to withstand an operating voltage of 14.4kV. Due to the series connection of the basic modules (see Fig.1) the required isolation voltage is increasing by 14.4kV per SPRC basic module. Hence, the last transformer in the series connection has to isolate the full output voltage of 115kV.

Fig.8 shows the partial discharge measurement setup. The transformer (DUT) is placed inside the oil tank where its primary is shorted and grounded via the metal plate. The secondary is also shorted and connected to the high voltage electrode inside the double toroid. This double toroid is used to compensate the different material intersections which could lead to additional external partial discharges. The whole setup is located in a Faraday cage and has a ground noise level without DUT of about 300fC. For optimal test conditions the oil has been processed through a filtration system resulting in a moisture level lower than 6ppm. To reduce possible partial discharges to a minimum, it is important to remove the air out of the DUT. Therefore, the oil tank has been filled under a pressure of 200mbar below atmospheric pressure. Further air reduction has been achieved by rotating the DUT within the oil. All measurements have been carried out at a room temperature of 23.5°C. The partial discharges Q are recorded with an Omicron MPD600 measurement system [18] and are evaluated according to the IEC 60270:2000 standard [19] leading to Q_{IEC}.

For a valid isolation design, the DUT has to pass the following test procedure. First, the nominal operation voltage ($115\mathrm{kV}/\sqrt{2} = 82\,\mathrm{kV_{RMS}}$ RMS, frequency $f = 50\mathrm{Hz}$) is applied as test voltage V_{test} to the DUT for 60 min. No breakthrough should occur and the partial discharge level Q_{IEC} should be below 2pC. Afterwards, V_{test} is increased stepwise up to a voltage of $110\,\mathrm{kV_{RMS}}$ (136%) with a test duration T_{Test} of 5min for each step. To pass the test, no breakthrough must occur. The DUT passed the first test with a Q_{IEC} value far lower than 2pC, as can be seen in Fig.9. Fig.10 shows a typical phase resolved discharge pattern which has been recorded during the green time interval in Fig.9(b). Most of the discharges occur at or near the positive or the negative half wave maximum of the test sinus. This could be interpreted

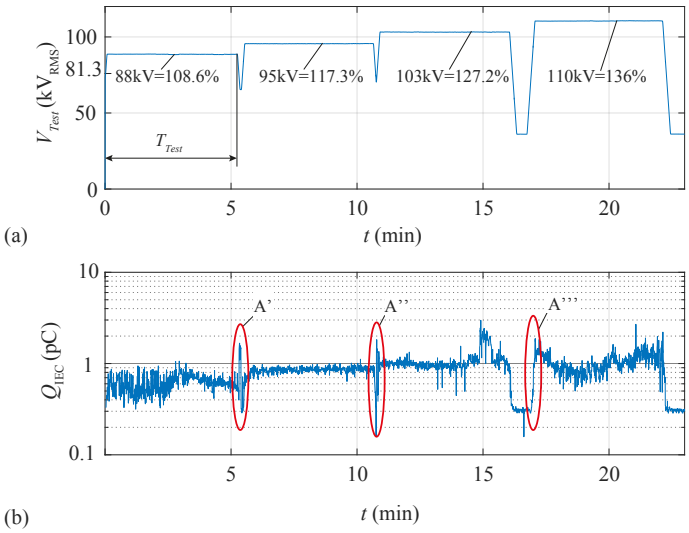

Fig. 11: (a) Stepwise increased stress voltage with a test interval $T_{Test} \geq 5$min and (b) averaged measured partial discharges level Q_{IEC} which has been weighted considering [19]. The peaks A',A" and A"' are caused by the main supply of the HV test transformer.

as a combination of corona and void or surface discharges with single ended contact to one electrode according to [10]. Also the second test is passed successfully as depicted in Fig.11. In the next step, V_{Test} is increased stepwise ($+9\%$) from $+100\%$ to $+136\%$ (see Fig.11(a)). There, also and no breakthrough occurred (see Fig.11(b)). The Q_{IEC} level still remains below 2pC for the first two voltage steps. The peaks in A', A" and A"' are caused by the variable ratio transformer which is the controlled primary main supply of the HV test transformer.

IV. Conclusion

In this paper, a comprehensive isolation design procedure for a 14.4kV nominal output voltage, 100kHz transformer with an isolation voltage of 115kV is presented. The procedure consists of a fast analytical maximum electrical field evaluation used during the automatic optimization of the transformer and a field conform post processing isolation design check. The resulting isolation system is verified by partial discharge measurements. First, a 60 min long test at nominal voltage is performed and afterwards the test voltage has been increased from 100% to 136% in 9% voltage steps. Each voltage step is applied for 5 min. Both tests are passed with no breakthroughs and the partial discharge level is lower then 2pC at nominal voltage. For long life times it is essential to remove the air from the transformer isolation system.

Acknowledgment

The authors would like to thank the project partners CTI and Ampegon AG very much for their strong support of the CTI-research project 13135.1 PFFLR-IW.

References

[1] M. Jaritz and J. Biela, "Optimal Design of a Modular Series Parallel Resonant Converter for a Solid State 2.88 MW/115-kV Long Pulse Modulator," *IEEE Transactions on Plasma Science*, no. 99, 2014.

[2] M. Jaritz, T. Rogg, and J. Biela, "Control of a modular series parallel resonant converter system for a solid state 2.88mw/115-kv long pulse modulator," in *17th European Conference on Power Electronics and Applications*, Sept 2015, pp. 1–11.

[3] J. Liu, L. Sheng, J. Shi, Z. Zhang, and X. He, "Design of High Voltage, High Power and High Frequency Transformer in LCC Resonant Converter," in *Applied Power Electronics Conference and Exposition.*, Feb 2009, pp. 1034–1038.

[4] J. C. Fothergill, P. W. Devine, and P. W. Lefley, "A novel prototype design for a transformer for high voltage, high frequency, high power use," *IEEE Transactions on Power Delivery*, vol. 16, no. 1, pp. 89–98, Jan 2001.

[5] T. Filchev, F. Carastro, P. Wheeler, and J. Clare, "High voltage high frequency power transformer for pulsed power application," in *Power Electronics and Motion Control Conference*, Sept 2010.

[6] Y. Du, S. Baek, S. Bhattacharya, and A. Q. Huang, "High-voltage high-frequency transformer design for a 7.2kV to 120V/240V 20kVA solid state transformer," in *36th Annual IEEE Industrial Electronics Society Conference*, Nov 2010, pp. 493–498.

[7] L. Heinemann, "An actively cooled high power, high frequency transformer with high insulation capability," in *Applied Power Electronics Conference and Exposition.*, vol. 1, 2002, pp. 352–357 vol.1.

[8] J. Biela and J. W. Kolar, "Using transformer parasitics for resonant converters—a review of the calculation of the stray capacitance of transformers," *IEEE Transactions on industry applications*, vol. 44, no. 1, pp. 223–233, 2008.

[9] http://www.midel.com, accessed Sep. 6, 2014.

[10] A. Küchler, *Hochspannungstechnik: Grundlagen - Technologie - Anwendungen*, ser. VDI-Buch. Springer, 2009.

[11] http://www.whm.net/content/de/download/res/14519-4.pdf, accessed May. 6, 2016.

[12] https://shop.maagtechnic.ch/maag/Datasheets/PC-Polycarbonate_eng.pdf, accessed May. 6, 2016.

[13] http://www.3dformtech.fi/lataukset/Material-Data-PA2200.pdf, accessed May. 6, 2016.

[14] http://www.roechling.com/de/hochleistungs-kunststoffe/duroplastische-kunststoffe/faserverstaerkte-kunststoffe/verbindungselemente.html, accessed May. 6, 2016.

[15] W. Kaddar, "Die generative Fertigung mittels Laser-Sintern: Scanstrategien, Einflusse verschiedener Prozessparameter auf die mechanischen und optischen Eigenschaften beim LS von Thermoplasten und deren Nachbearbeitungsmoglichkeiten," Ph.D. dissertation, Duisburg, Essen, Univ., Diss., 2010.

[16] F. Derler, H. Kirch, C. Krause, and E. Schneider, "Development of a Design Method for Insulating Structures Exposed to Electric Stress in Long Oil Gaps and along Oil/Transformerboard Interfaces." 7th Int. Symp. on High Voltage Engineering, 1991.

[17] H. P. Moser, V. Dahinden, and H. Friedrich, *Transformerboard: die Verwendung von Transformerboard in Grossleistungstransformatoren*. Basel: Birkhäuser, 1979.

[18] https://www.omicronenergy.com/de/products/all/primary-testing-monitoring/mpd-600, accessed May. 6, 2016.

[19] *IEC 60270:2000 VDE 0434:2001-08: "High-voltage test techniques - Partial discharge measurements"*, Std., Genf, 2000.